Eur. Phys. J. Plus (2024) 139:900
https://doi.org/10.1140/epjp/s13360-024-05678-y

THE EUROPEAN PHYSICAL JOURNAL PLUS

Regular Article

Neutron spectrometry of a ^{241}Americium-Boron neutron source using the NCT-WES single-moderator neutron spectrometer

R. Bedogni[1], L. Russo[1], A. I. Castro Campoy[1,2], M. A. Caballero-Pacheco[1], D. Dashdondog[1,2], T. Napolitano[1], M. Del Franco[1], A. Calamida[3], S. Loreti[3], F. Moro[3], Antonino Pietropaolo[1,3,a]

[1] Istituto Nazionale di Fisica Nucleare - Frascati National Laboratories, Frascati, Italy
[2] Centro Internazionale di Fisica Teorica Abdus Salam (ICTP), Trieste, Italy
[3] ENEA- Department of Fusion and Technologies for Nuclear Safety and Security, Frascati, Italy

Received: 5 July 2024 / Accepted: 21 September 2024

Abstract ^{241}Americium-boron (α,n) neutron sources have been produced for various application from nuclear industry to well logging or radiation protection. Compared to ^{241}Americium–beryllium sources their specific emission rate is lower, but their spectrum is narrower, and their production cycle uses boron, which is less toxic than beryllium. Very few data are available in literature about the energy distribution of this neutron source: the 2001 version of Standard ISO 8529-1 reported a reference spectrum derived from 1970s data, exhibiting a single peak from about 1 to 6 MeV. Other spectra are available in recent works from PTB and NPL, based on high-resolution spectrometers and Bonner spheres. ENEA Frascati owns a ^{241}Am-B neutron source with nominal emission rate 3.5×10^6 s^{-1}. Knowing its spectrum is important, as this source is used to feed the HOTNES (Homogeneous Thermal Neutron Source) facility. A spectrometry experiment was organized relying on the recently developed NCT-WES neutron spectrometer. Belonging to the family of the Single Moderator Neutron Spectrometers, NCT-WES is a convenient alternative to Bonner spheres as it derives the whole spectrum from a single exposure. The experimental data were elaborated in comparison with the existing literature spectra. As a main results of the study, the spectrum of the ENEA ^{241}Am-B neutron source nearly perfectly agrees with that derived at NPL.

1 Introduction and state of art

Radionuclide neutron sources based on (α,n) reactions are employed in a variety of fields including reactors, density and humidity gauging, well-logging, activation analysis, radiation protection and industry [1]. They usually consist of a compacted mixture of the oxide of the α-emitting nuclide with a target material [2]. Due to its long half-life (432 y), ^{241}Am is usually preferred as α-emitting nuclide. ^{9}Be is the most used target material, as its neutron separation energy (1.67 MeV) is the lowest among stable nuclides. Consequently, (α,n) sources based on beryllium have the highest specific emission rate (6.6×10^{-5} s^{-1} Bq^{-1} for ^{241}Am-Be). ^{241}Americium–boron (α,n) neutron sources are also used. Their specific emission rate, about 1.6×10^{-5} s^{-1} Bq^{-1}(^{241}Am), is four times lower than that of ^{241}Am-Be. Consequently, larger capsules are needed to obtain modest emission rates. However, their production cycle is less hazardous, as boron is less toxic than beryllium. In addition, their spectrum, extending from 1 to 6 MeV, is considerably narrower than ^{241}Am-Be, spanning from 0.1 to 11 MeV.

Very few data are available in literature about the spectrum of the ^{241}Am-B neutron source. The first modern spectrometry study of the ^{241}Am-B spectrum was done by Lorch [2] using a thin stilbene scintillator with pulse shape discrimination technique and covered the energy interval from about 1 to 6 MeV. The spectra reported in the 1989 and 2001 versions of the ISO Standard [3, 4] and in the IAEA Technical Report Series 318 [5] were derived from this spectrum, but they exhibit additional energy bins below 1 MeV whose origin is unknown. Thus, for the purposes of this work, only the original Lorch spectrum was considered. More recent spectra were obtained at PTB with a liquid NE213 scintillator [6] and at NPL with a ^{3}He sandwich spectrometer [7] combined with Bonner spheres (BS) and calculations with the codes MCNP and SOURCES 4C [8]. The Lorch, PTB and NPL spectra are compared in Fig. 1. These are lethargy plots reporting the quantity $\Delta\Phi_i/\Phi/\ln(E_{i+1}/E_i)$, where $\Delta\Phi_i$ is the fluence in the i-th energy interval, Φ the total fluence, and E_i is the lower limit of the i-th energy interval. This representation is the one adopted in the ISO Standard 8529–1 [9]. These literature spectra are defined in the following energy intervals: NPL, from 7 eV to 20 MeV; PTB, from 1.6 MeV to 20 MeV; Lorch, from 1 MeV to 6.2 MeV.

As the PTB spectrum is only given above 1.6 MeV, all spectra have been normalized to have the same fluence above 1.6 MeV. NPL and PTB spectra are comparable and both exhibit a peak at higher energy than Lorch. The spectral information below 1.6 MeV

[a] e-mail: antonino.pietropaolo@enea.it (corresponding author)

Published online: 16 October 2024

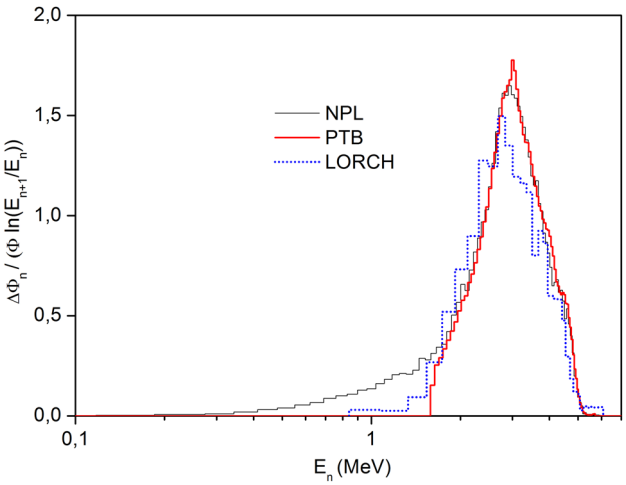

Fig. 1 Lethargy plots of the NPL, PTB and Lorch spectra for the ^{241}Am-B neutron source. All spectra have been normalized to have the same fluence above 1.6 MeV

Table 1 Constructive details of the sources

Data set	Capsule	Emission rate s^{-1}	Diameter (mm)	Height (mm)	Cylindrical wall thickness (mm)	End caps thickness (mm)
Lorch	X3	5×10^5	22.4	31.0	2.3	5.0, 3.2
NPL	X3	4.4×10^5	22.4	31.0	2.3	5.0, 3.2
PTB	X2	1.506×10^5	17	19		
ENEA	X14	3.5×10^6	30	60	2.2	5.0, 3.3

The active material of the Lorch source was formed by 12 g natural B + 0.35 g AmO_2 in pellets pressed to 4 tons [2]

in the NPL spectrum comes from the MCNP / SOURCES 4C simulations combined with BS measurements [8]. The nominal characteristics of the ^{241}Am-B sources used in the Lorch, NPL and PTB works are listed in Table 1.

ENEA Frascati owns a ^{241}Am-B neutron source with nominal emission rate 3.5×10^6 s^{-1}. Its nominal characteristics are also reported in Table 1. A detailed knowledge of its spectrum is important, as it is currently used to feed the HOTNES (Homogeneous Thermal Neutron Source) facility [10–12]. As this source is about one order of magnitude more intense than the other sources in Table 1, it includes more active material. An interesting part of this work is investigating whether the scattering effects due to the augmented amount of material can cause spectral variations with respect to the smaller sources. A similar approach applied to ^{241}Am-Be sources of different types allowed obtaining the "large" and "small" spectral qualities reported in the current version of ISO Standard 8529–1 [9]. The spectrometric measurements of the ENEA source were performed using the recently developed NCT-WES single moderator neutron spectrometer, briefly explained in Sect. 2.

2 The NCT-WES single moderator neutron spectrometer

Belonging to the family of the Single Moderator Neutron Spectrometers (SMNS) [13–16], NCT-WES is a convenient alternative to Bonner Spheres.

Although details on this instrument are given elsewhere [17, 18], its main features are recalled here for reader's sake. Overall, NCT-WES is a high-density polyethylene (HDPE) cylinder with 36 cm diameter and 41.5 cm height, see a cut view in Fig. 2 It is formed by three main fitting pieces: the collimator, the sensitive capsule and the external shielding. Thanks to the external shielding made of HDPE and borated rubber, the internal sensors only "see" the neutrons coming from the cylindrical collimator. This has length 20 cm, diameter 11 cm and is internally lined with 0.5 cm of borated rubber. The sensitive capsule embeds six nominally identical thermal neutron detectors at different depths along the cylindrical axis of the device. Each detector is a windowless p−i−n diode featuring 1-cm^2 area, 300 μm thickness and coated with 30 μm of ^{6}LiF. Detectors are acquired by means of a spectroscopy chain formed by charge preamplifiers and shaper amplifiers. The thermal neutron pulses are discriminated from the gammas and the electronic noise by applying a threshold in terms of pulse height (0.6 V) [19, 20].

The centres of the thermal neutron detectors are located along the cylindrical axis at different distances from the spectrometer front face, namely: 20.22 (shallowest detector in position P1), 21.52, 22.82, 24.12, and 26.12 and 28.12 cm (deepest detector in position P6). Air penetrations in the sensitive capsule were designed to enhance the epithermal response of deeper detectors.

As explained in Ref. [21]:

- The device was fully modelled with MCNP [22];

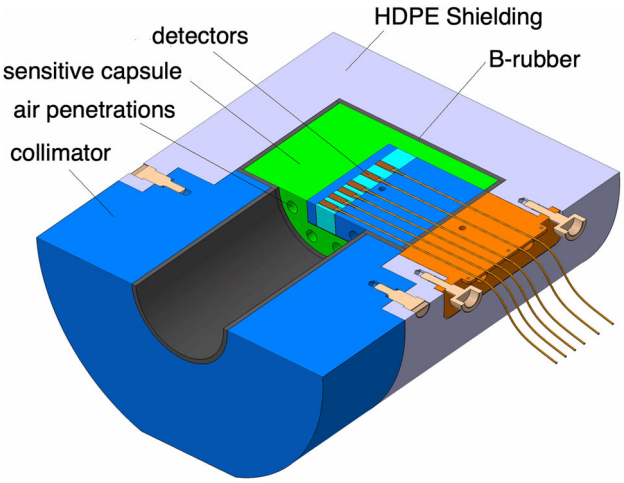

Fig. 2 Cut view of NCT-WES

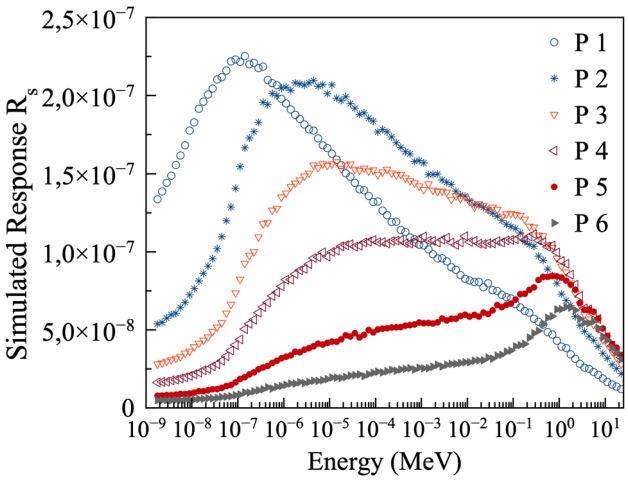

Fig. 3 Simulated response matrix of NCT-WES in terms of number of counts in the i-th sensor per emitted neutron, as a function of the neutron energy, when the spectrometer is exposed to an isotropic volume source located at 151.5 cm from its front face. Symbols P1 to P6 indicate the detector positions from the shallowest to the deepest

- The signal in the internal thermal neutron sensors is regarded as proportional to a Monte Carlo estimator that is the number of (n,t) reactions in the ^{6}LiF radiator;
- The experimental number of pulses in the sensors is obtained by multiplying this Monte Carlo estimator by a previously estimated scaling factor, $F = (0.238 \pm 0.006)$ pulses/ (n,t) reaction [17].
- The NCT-WES Monte Carlo model was experimentally validated using monoenergetic and continuous spectrum reference fields [17, 21], and its overall uncertainty was found to be lower than $\pm 2\%$ in the energy domain from few tens of keV up to the spectrum of ^{241}Am-Be (maximum energy 11 MeV).
- Due its large size, its directionality and the presence of multiple sensors distributed over a length of about 8 cm, NCT-WES response matrix not only depends on the energy and the detector position, but also on the irradiation geometry. In this work the irradiation geometry consisted in an isotropic volume source which centre was located at 151.5 cm from the spectrometer front face. Under this condition, a workplace-specific response matrix $R_s(E,i)$ was calculated, where "i" represents the detector position from P1 (shallowest) to P6 (deepest). Thus, $R_s(E,i)$ is the number of counts in the i-th sensor per emitted neutron, as a function of the neutron energy, when the spectrometer is exposed to an isotropic volume source located at 151.5 cm from its front face. See Fig. 3.

It should be remarked that for neutron metrology purposes, as in this work, NCT-WES is more convenient than Bonner Spheres (BS) for two reasons:

- NCT-WES requires considerably less measurement time than BS. In a previous collaboration with STUK (Finland), NCT-WES needed only five days to characterize two ^{252}Cf and two ^{241}Am-Be sources with emission rate from 2×10^6 to 2×10^7 s^{-1} [23].
- Due to its directional response, NCT-WES is considerable less sensitive to room-scattered radiation than BS.

3 Experiment

The experiment took place in the low scatter room of the ENEA Frascati Neutron Generator [24]. The setup is shown in Fig. 4. The spectrometer was allocated at 1.75 m from ground on top of a specially designed steel holder with 2-axis rotation capability. The distance from the concrete walls was at least 6 m. To determine the room-scatter contribution to the detector readings, a HDPE cylindrical shadow-bar with diameter and height 40 cm was interposed between the source and the detector at 40 cm from the source. The discussion about the shadow bar is presented below.

The scatter-free count rates of the detectors were determined by subtracting the "shadow-bar" count rate from that obtained in free-field condition, i.e. without bar.

The irradiation time was 17 h for the free-field and 6 h for the shadow-bar measurement. The scattered fraction, here defined as the quotient between the shadow-bar and the free-field count rate, varied between 15% for detector P1 (shallowest) to 9% for detector P6 (deepest). For Bonner Spheres at similar distance this ratio would easily increase to > 40% [25]. After correcting for room-scatter, the net count rate in the NCT-WES detectors ranged from about 0.10 (s.d. 1.6%) to 0.21 s^{-1} (s.d. 1%). The plot of the net count rate as a function of the detector position follows a continuous behaviour with a maximum in position P4, as shown in Fig. 5. The same figure also reports the free-field and shadow-bar profiles.

The shadow-cone or shadow-bar procedures, used to measure the room-scatter contribution to an instrument reading, are influenced by the following "shadowing parameters", to be considered in relation to the instrument size and its distance from the source:

- the source-to-attenuator distance;
- the attenuator geometry: in our case the diameter of the bar and its length.

If the attenuator is too close to the source, it may lead to underestimate the scattered contribution. If the attenuator does not obscure the whole instrument solid angle, it may lead to overestimate the scattered contribution. If the attenuator it too thin, it may also lead to overestimate the scattered contribution. If the shadowing parameters are well-chosen, the experimental net count rate (free-field minus shadow) should coincide, within a pre-fixed uncertainty budget, with the "idealised" scatter-free count rate (ideally obtained in a room with no air and no walls). For the current experiment the shadowing parameters, chosen by Monte Carlo simulations, allowed matching this requirement by 2% or less. This is described below.

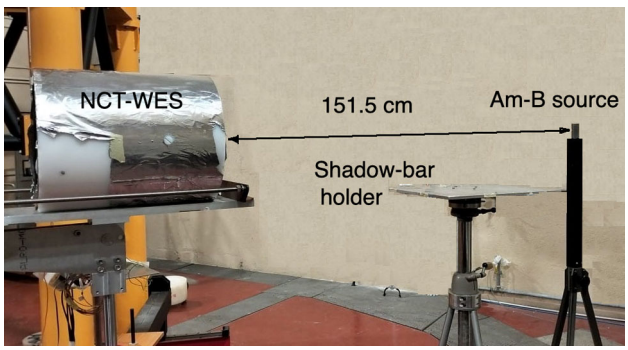

Fig. 4 Irradiation setup including the spectrometer, the source and their holders. In addition, the shadow-bar holder is shown

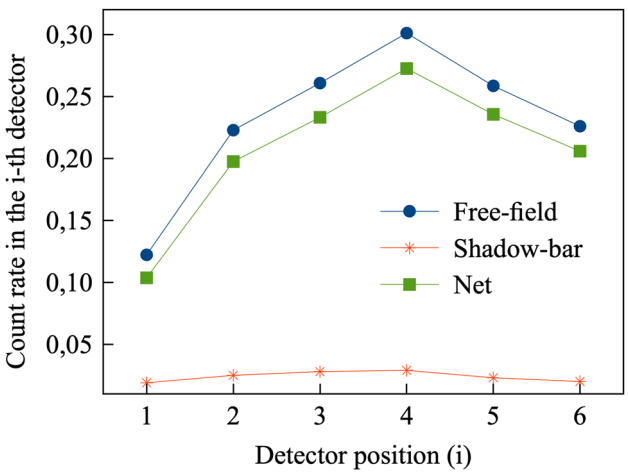

Fig. 5 Count rates of the NCT-WES internal detectors for the free-field, shadow-bar and net conditions

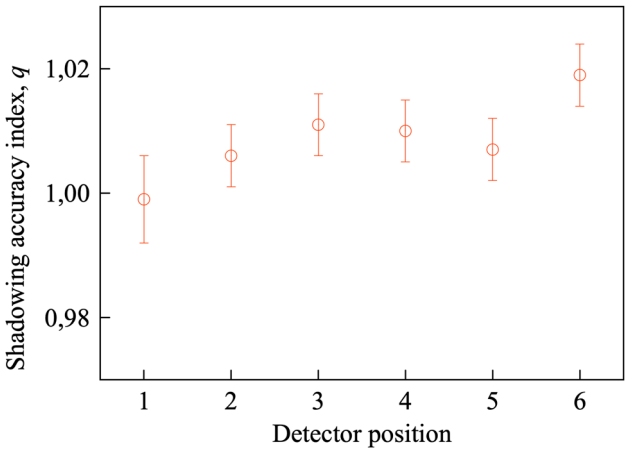

Fig. 6 Shadowing accuracy index for the various detector positions, 1 being the shallowest and 6 the deepest

An MCNP simulation was performed including detailed models of the FNG hall, the source and the instrument. Figure 6 shows the *shadowing accuracy index*, q, for the various detector positions, defined as follows:

$$q = \frac{n_{exp} \times e^{\Sigma \times d}}{n_{ideal}} \tag{1}$$

where:

- n_{exp} is the simulation of the experimental net count rate, i.e. the difference between the simulated readings in absence and in presence of shadow-bar;
- $\sum$ is the linear attenuation coefficient of the air, based on the total neutron cross section of its constituents averaged over the spectral neutron distribution of the source. For ^{241}Am-B this value is 8.33×10^{-5} cm^{-1} [26];
- d is the source-to-detector distance;
- the factor $e^{\Sigma \times d}$, henceforth named F_{air}, is the air attenuation correction factor and its numerical value is 1.013.
- n_{ideal} is the simulation of the "idealised" scatter-free count rate, obtained by removing the FNG hall and the air from the simulation.

As shown in Fig. 6, the q deviations from unity are comparable with the uncertainties of the experimental net count rates ($\pm 1.6\%$, one s.d., or less), thus the shadowing method does not significantly bias the experiment.

4 Data processing

As shown in Sect. 1, there are basically three literature spectra for the ^{241}Am-B source, all of them based on nuclear recoil spectrometers, and referred to as Lorch (in its original formulation), PTB and NPL spectra. As pointed out by Thomas [27], integral spectrometers like BS (or SMNS) have superior energy interval of response and easier operation than nuclear recoil devices, but they have inferior energy resolution. This disadvantage comes from the shape of the response functions of different spheres (or, for NCT-WES, different internal detectors), which exhibit overlapping and similarities. Therefore, this work does not pretend to produce a ^{241}Am-B spectrum with better energy details then the cited high-resolution spectra. Instead, objectives of this work are:

(1) Determining the emission rate of the ENEA ^{241}Am-B source;
(2) Evaluating which high-resolution literature spectrum best represents the ENEA source.

4.1 Determining the emission rate of the ENEA ^{241}Am-B source

The literature on integral spectrometers like BS [27, 28] or SMNS [16] claims that these instruments can estimate the total fluence (or the emission rate, in case of SMNS) with high accuracy (better than $\pm 5\%$), independently of the quality of the pre-information provided to the unfolding code. Mandatory requisites to achieve this target are:

- Data are acquired with good counting statistics;
- The instrument is accurately modelled and the response matrix is verified in reference fields;
- The unfolding code is provided with accurate pre-information on the energy domain. In other words, unfolding codes do not add neutrons in energy domains that are not comprised in the pre-information.

On this ground, the NCT-WES data were unfolded with the FRUIT unfolding code in "special gradient mode" [29, 30], using the NPL spectrum as pre-information. All results from different unfolding procedures will be shown and discussed in Sect. 4.3. As NPL spectrum was derived from a combination of high-resolution and BS data, it includes a low-energy component down to few eV.

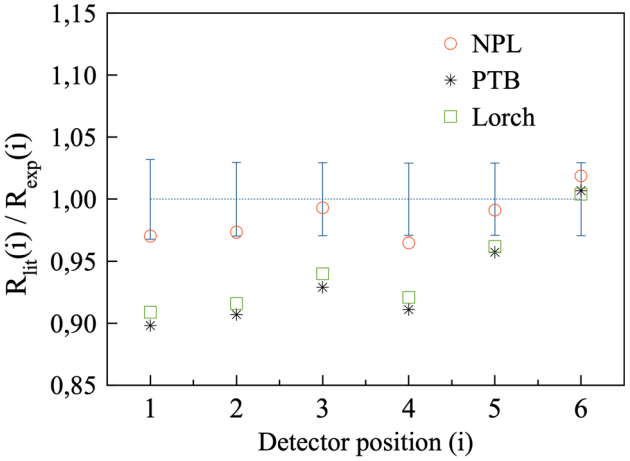

Fig. 7 Ratio R_{lit}(i) / R_{exp}(i) for the different detector positions and the Lorch, PTB and NPL spectra. For a better readability, the uncertainty on the ratio (around $\pm 3\%$) is shown as a boundary around one

To minimise discretization errors, NCT-WES response matrix was calculated using the same energy structure of the NPL spectrum. The unfolded "apparent" emission rate of the source is $B_a = (3.43 \pm 0.11) \times 10^6$ s^{-1}, where "apparent" means not including the air attenuation and assuming a perfect isotropic emission. The best estimation of the source emission rate, B, is thus given by:

$$B = \frac{B_a}{\mathrm{F}_{90^\circ}} \times F_{air} = (3.36 \pm 0.11) \times 10^6 \text{ s}^{-1} \tag{2}$$

where:

- F_{90° is the anisotropy factor of the source in the direction used for the measurement (indicated as 90°). Having no experimental information on this factor, the literature value of 1.0345 ± 0.0054, measured for the NPL source [31], was used.
- F_{air} is the air attenuation correction factor derived in Sect. 3.

4.2 Which literature spectrum best represent the ENEA source?

A direct method to choose which literature spectrum best represents the ENEA source is to compare the experimental net count rates with those expected from the different literature spectra. The experimental data is R_{exp}(i), i.e. the quotient between the experimental net count rate of the i-th detector and the measured source emission rate. The corresponding "expected" quantity for a given literature spectrum is:

$$R_{lit}(i) = \int_0^\infty dE \times \varphi_{lit}(E) \times R_s(E,i) \tag{1}$$

where:

- R_{lit}(i) represents the counts of the i-th detector per unit emission rate expected from a given literature spectrum;
- $\varphi_{lit}(E)$ is the literature spectrum normalised to unit fluence (unit spectrum);
- R_s(E,i) is the NCT-WES response matrix as defined in Sect. 2, where "i" refers to the i-th detector.

To minimise discretisation errors, all literature spectra were re-binned to the energy structure of the NPL spectrum.

Figure 7 reports the ratio R_{lit}(i) / R_{exp}(i) for the different detector positions and the Lorch, PTB and NPL spectra. For a better readability, the uncertainty on the ratio (around $\pm 3\%$) is shown as a boundary around the unity.

As the PTB and Lorch spectra do not have neutrons below respectively 1.6 and 1 MeV, the corresponding profiles are considerably lower than unity for the most superficial detectors. As deeper sensors are less sensitive to low-energy, these profiles tend to unity for deeper positions (P5 and P6). The NPL profile is always very near to unity, indicating that the ENEA source and NPL spectra are basically compatible, within the limits of the energy resolution of NCT-WES.

4.3 Unfolding exercise

According to the profiles shown in Sect. 4.2, the NPL spectra satisfactorily reproduces the experimental NCT-WES counts. The Lorch and PTB spectra, as expected, need an additional low-energy component. The shape of such low-energy component can be only investigated via unfolding. Thus, three unfolding sessions were performed, using three different guess spectra:

(1) the NPL spectrum;
(2) the PTB spectrum combined, for the energy domain below 1.6 MeV, with the NPL one (called PTB-NPL mix)
(3) the Lorch spectrum combined, for the energy domain below 1 MeV, with the NPL one (called Lorch-NPL mix).

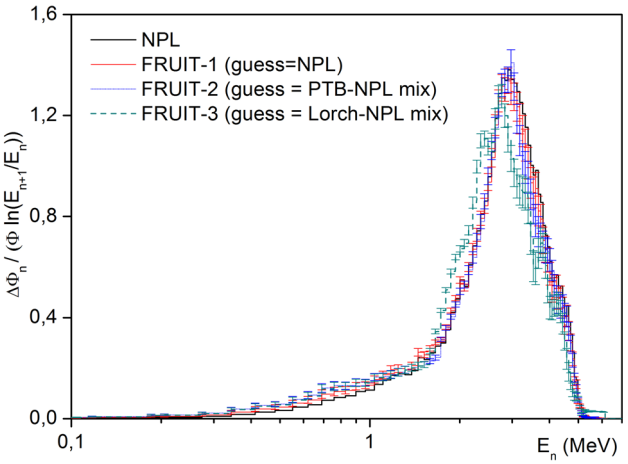

Fig. 8 ENEA source unfolded spectra using three different guess spectra: (1) the NPL spectrum (2) the PTB-NPL mix, (3) the Lorch-NPL mix

Table 2 Relevant spectrum-integrated quantities for the four spectra reported in Fig. 8 plus the Am-B spectrum from the 2001 version of ISO Standard 8529-1 [4]

	ISO 2001	NPL	FRUIT-1	FRUIT-2	FRUIT-3
h*(10) (pSv cm^2)	408	410	407 ± 8	404 ± 8	406 ± 8
Fluence average energy (MeV)	2.72	2.72	2.63 ± 0.05	2.58 ± 0.05	2.49 ± 0.05
Ambient dose equivalent average energy (MeV)	2.8	2.73	2.65 ± 0.05	2.62 ± 0.05	2.52 ± 0.05

h*(10) is the spectrum-average fluence-to-ambient dose equivalent conversion coefficient

In such a way, the low-energy portion of the NPL spectrum was proposed as a common low-energy component in all unfolding sessions. Indeed, unfolding is an under-determined process and the guess spectrum should be formulated by including every available piece of pre-information. In this case, the low-energy portion of the NPL spectrum was regarded as reliable pre-information, as it was derived from measurements and simulations based on physical models. Data were unfolded by means of the FRUIT unfolding code in "special gradient mode". The unfolded spectra are shown in Fig. 8.

Uncertainties in Fig. 8 are specified on a bin-per-bin basis and are obtained by propagating uncertainties on the input quantities (response matrix and sensors counts) through the unfolding process [30, 32]. Interestingly, the original NPL spectrum coincides with the unfolded spectra obtained using, as guess spectra, the original NPL (FRUIT-1) or PTB-NPL mix (FRUIT-2). The unfolded spectrum based on the Lorch-NPL mix (FRUIT-3) is close to them, but it peaks at slightly lower energy. The unfolded spectra FRUIT-1, FRUIT-2 and FRUIT-3 have similar degrees of coherence with the experimental count rates. FRUIT quantifies this parameter using the "Average Detector Deviation" (ADD). For a given NCT-WES internal detector, the "Detector Deviation" (DD) is the difference between the experimental count and that obtained by folding the response function of that detector with the unfolded spectrum. ADD is the average of DD over the six internal detectors and its values, for all unfolded spectra, is 1% or lower.

It should be noted that all the unfolded spectra feature a slightly higher emission in the region below 1 MeV, as compared to the original NPL spectrum. As the ENEA source includes more active material than the NPL source, this could be ascribed to neutron scattering in the active material. The same was observed when comparing the spectra from ^{241}Am-Be sources with different capsules and amounts of active material [33, 34].

The three unfolded spectra were used to re-calculate the source emission rate, and all results agree within 2% with the value derived in Sect. 4.1.

Table 2 presents relevant spectrum-integrated quantities for the four spectra reported in Fig. 8 plus the Am-B spectrum reported in the 2001 version of ISO Standard 8529–1 [4]. The higher fraction of low-energy neutrons in the ENEA spectrum (FRUIT-1, FRUIT-2 and FRUIT-3), if compared to the NPL spectrum, causes slightly lower values for these spectrum-integrated values.

5 Conclusions

The ENEA Frascati ^{241}Am-B, having nominal emission rate 3.5×10^6 s^{-1}, was studied using the NCT-WES single moderator neutron spectrometer. Three relevant literature spectra, from Lorch, PTB and NPL, were considered as terms of comparison. Whilst NPL spectrum is defined down to 7 eV, the PTB and Lorch spectra have 1.6 MeV and 1 MeV as low-energy limits. Relying on the FRUIT unfolding code, the following characteristics were investigated:

(1) the neutron emission rate was measured with uncertainty 3.3%;

(2) among the available literature spectra, the NPL one is the most coherent with the experimental data for the ENEA source.
(3) the unfolded spectra FRUIT-1 and FRUIT-2 are very close to the original NPL spectrum, but they exhibit slightly higher emission in the region below 1 MeV. As the ENEA source includes more active material than the NPL source, this could be ascribed to neutron scattering in the active material.
(4) The unfolded spectrum (FRUIT-3) based on the Lorch-NPL mix is close to the other spectra of Fig. 8, but it peaks at slightly lower energy.
(5) All unfolded spectra provide the same source emission rate within the uncertainties.
(6) Relevant spectrum-integrated quantities are reported for all the elaborated spectra.

To conclude, this work measured, for the first time, the neutron spectrum from a "large" ^{241}Am-B source. The results are coherent with a spectrum measured at NPL for a smaller source [8]. However, limited spectral effects tend to appear in the low-energy domain. These are possibly due to the larger amount of active material compared to the NPL source.

Acknowledgements The research presented in this paper has been partially financed by the projects ENTER_BNCT (Commissione Scientifica Nazionale CSN5 of INFN) and SORGENTINA (ENEA). D. Dashdondog and A.I. Castro Campoy are funded by the TRIL (Training and Research in Italian Laboratories) program of the Centro Internazionale di Fisica Teorica Abdus Salam (ICTP), Trieste (Italy). The numerical values of the PTB and NPL spectra reported in Fig. 1 were kindly provided by A. Zimbal (PTB) and N. Roberts (NPL), respectively.

Funding Open access funding provided by Ente per le Nuove Tecnologie, l'Energia e l'Ambiente within the CRUI-CARE Agreement.

Data Availability Statement Data will be made available on reasonable request. The manuscript has associated data in a data repository.

Declarations

Competing interests The authors declare no conflict of interest.

References

1. National Research Council, *Source Use and Replacement: Abbreviated Version* (The National Academies Press, Washington, DC, 2008)
2. E.A. Lorch, J. Appl. Radiat. Isot. **24**, 585 (1973)
3. ISO, Neutron reference radiations for calibrating neutron-measuring devices used for radiation protection purposes and for determining their response as a function of neutron energy. ISO 8529 (1989).
4. International standard ISO 8529–1. ISO (2001).
5. IAEA: Compendium of neutron spectra and detector responses for radiation protection. TRS 318 (1990).
6. A. Zimbal, Radiat. Prot. Dos. **126**, 413 (2007)
7. J.W. Marsh, D.J. Thomas, M. Burke, Nucl. Instr. Meth. A **366**, 340 (1995)
8. N.J. Roberts et al., Rad. Prot. Dosim. **161**, 225 (2014)
9. ISO, International Standardization Organization, Neutron Reference Radiation fields - Part 1: Characteristics and Methods of Production. ISO 8529–1:2021 (2021)
10. R. Bedogni et al., Appl. Rad. Isotop. **127**, 68 (2017)
11. A. Sperduti et al., JINST **12**, P12029 (2017)
12. R. Bedogni et al., Nucl. Instr. Meth. A **843**, 18 (2017)
13. R. Bedogni et al., Nucl. Instrum. Methods A **782**, 35 (2015)
14. R. Bedogni et al., Nucl. Instrum. Methods A **927**, 151 (2019)
15. R. Bedogni et al., Europhys. Lett. **127**, 12002 (2019)
16. A. Pietropaolo et al., Phys. Rep. **875**, 1 (2020)
17. R. Bedogni et al., Europhys. Lett. **134**, 42001 (2021)
18. Bedogni et al., Eur. Phys. J. Plus **137**, 773 (2022)
19. R. Bedogni et al., Nucl. Instrum. Methods A **780**, 51 (2015)
20. R. Bedogni et al., Nucl. Instr. Meth. A **1018**, 165855 (2021)
21. R. Bedogni et al., Eur. Phys. J. Plus **138**, 270 (2023)
22. C. J. Werner (Ed.), MCNP Users'Manual Code Version 6.2, Report LA-UR-17–29981, Los Alamos National Laboratory (USA, 2017).
23. R. Bedogni et al., Eur. Phys. J. Plus **139**, 384 (2024)
24. A. Pietropaolo et al., J. Phys. Conf. Ser. **1021**, 012004 (2018)
25. Establishing neutron calibrations at SSDL using ISO 8529. Online training course (2020).
26. ISO, International Standardization Organization, Neutron Reference Radiation fields - Part 2: Part 2: Calibration fundamentals of radiation protection devices related to the basic quantities characterizing the radiation field. ISO 8529–2:2000 (2000).
27. D.J. Thomas, Rad. Prot. Dosim. **110**, 141 (2004)
28. A.V. Alevra, D.J. Thomas, Radiat. Prot. Dosim. **107**, 37 (2003)
29. R. Bedogni et al., Nucl. Instr. Meth. A **580**, 1301 (2007)

30. K. Amgarou et al., Nucl. Inst. Meth. A **654**, 399 (2011)
31. A.G. Bardell, M. Burke, J.B. Hunt, D.J. Thomas, Anisotropy of emission from radionuclide neutron sources. NPL Report CIRM 24 (1998).
32. S. Agosteo et al., Nucl. Instr. Meth. A **694**, 55 (2012)
33. D.J. Thomas et al., Radiat. Prot. Dosimetry **180**, 21 (2018)
34. R. Bedogni et al., Nucl. Instr. Meth. A **763**, 547 (2014)